Chirp backscattering by pec sphere eccentrically placed in a dielectric sphere

Dimitrios Chrissoulidis, Elodie Richalot, Stéphane Protat

Chirp Backscattering by pec Sphere Eccentrically Placed in a Dielectric Sphere

Dimitrios Chrissoulidis[a,*], Elodie Richalot[b], Stéphane Protat[b]

[a] *Department of Electrical and Computer Engineering, Faculty of Engineering, Aristotle University, GR-54124 Thessaloniki, Greece*
[b] *ESYCOM Lab., Univ. Gustave Eiffel, UMR CNRS 9007, F-77454 Marne-la-Vallée, France*

Abstract

A plane electromagnetic (em) wave, amplitude- and frequency-modulated as a linear chirp, is incident on a dielectric sphere that hosts an eccentric, spherical, pec (perfect electric conductor) inclusion. This radiation problem is solved in the frequency domain by use of symmetry-dependent, spherical eigenvectors, the end-result being a set of linear equations for the wave amplitudes of the frequency spectrum of the electric field in every part of space. That set is solved by truncation and matrix-inversion, separately for even- and odd-symmetry wave amplitudes. The backscattered chirp is found by an inverse Fourier transform that yields the time-dependent, monostatic, radar cross section (mrcs). A numerical application manifests the possibility to detect a pec sphere concealed in an acrylic sphere by use of a wide-band chirp that targets a morphology-dependent resonance (mdr) of the composite body. Our theory and code are validated by use of a commercial software.

Keywords: `Pulse Scattering, Chirp, Eccentric Spheres`

2020 MSC: 00-01, 99-00

*Corresponding author

Email addresses: `dpchriss@auth.gr` (Dimitrios Chrissoulidis), `elodie.richalot@u-pem.fr` (Elodie Richalot), `stephane.protat@univ-eiffel.fr` (Stéphane Protat)

1. Introduction

Scattering of a modulated, plane, em wave by a non-spherical body is a radiation problem that finds several important applications. Among them, of current interest are: (a) non-destructive tests aimed at the detection of fabrication imperfections (e.g., cavities in artificial objects), (b) standoff detection of concealed items by microwaves (e.g., in security checkpoints), (c) non-invasive diagnoses of anomalies in the human body (e.g., tumors, gallstones etc.), and (d) real-time analysis of human breath gases by use of laser pulses.

"Non-spherical" [1] is a body that lacks spherical symmetry even though it is defined by several spherical interfaces (e.g., an eccentrically layered sphere, an aggregate of spheres, and combinations thereof). Lorenz-Mie [2, 3, 4, 5] solutions to scattering by non-spherical bodies have been formulated in the asymptotic case of continuous-wave (cw) – i.e., time-harmonic – excitation by use of the T-matrix method [6, 7, 8, 9, 10], IMM (indirect mode-matching) equations [11, 12, 13, 14, 15], and dyadic Green's functions [16, 17, 18]. Numerical solutions are available [19], too, but they are beyond the interest of this paper.

Amplitude modulation of the incident wave has been considered by a few researchers [20, 21, 22, 23] and by the first author in a previous paper [24]. The latter dealt with a dielectric sphere containing an eccentric spherical cavity. Developing that theory, we consider in this paper double modulation – amplitude and phase – of the incident wave in search of wide-band coupling to a non-spherical body. We study a dielectric sphere with an eccentric, spherical, pec inclusion exposed to a linear chirp having bandwidth-to-carrier ratio in excess of 25%. Our frequency-domain analysis results in the frequency spectrum of the backscattered electric field. The latter is subsequently used to determine the backscattered chirp that is associated with the time-dependent mrcs [25]. The envelope of the backscattered chirp is shown to carry wide-band information about the scatterer, which can be used to reveal the presence of a metallic inclusion in the host sphere.

2. Geometry and excitation

The geometry (Fig. 1) is quite simple: a non-magnetic, dielectric sphere in free space (region 0, wave-number $k_0 = \omega\sqrt{\epsilon_0\mu_0}$) accommodates a pec sphere. The host (region 2, wave-number $k_2 = \mathrm{n}_2 k_0$, radius a_2) is centred at O. The refractive index n_2 may be a complex number to account for eventual losses in the host. The inclusion (region 1, radius $a_1 < a_2$) is centred at O_1. The coordinates of O_1 in $(O, r\theta\phi)$ are $r = d_1 = |\mathbf{d}_1|, \theta = \Theta_1, \phi = \Phi_1$. The inclusion may be anywhere within the host. Hence, $d_1 + a_1 \leq a_2$ or $d_1 \leq d_{1,\max} = a_2 - a_1$. A field point may be defined by reference to the system of spherical coordinates $(O; r\theta\phi)$ or $(O_1; r_1\theta_1\phi_1)$, attached severally to the host sphere or the inclusion. The position vectors $\mathbf{r}$ and $\mathbf{r}_1$ are linked through $\mathbf{r} = \mathbf{d}_1 + \mathbf{r}_1$.

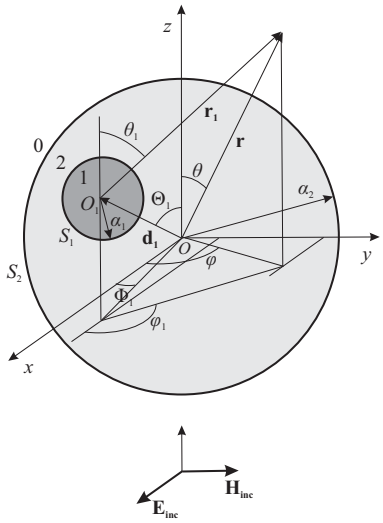

Figure 1: Non-spherical body: a number is assigned to each part of space: 0 (free-space), 1 (spherical pec inclusion), and 2 (dielectric host sphere).

Excitation is provided by a plane, em wave that is propagated in the direction $\hat{z}$ and polarised in the direction $\hat{x}$ (the unit vectors along x, y, z are $\hat{x}, \hat{y}, \hat{z}$). The electric-field vector of the incident wave is $\mathbf{E}_{\mathrm{inc}}(\mathbf{r}, t) = E(\tau)\exp\{j\omega_c\tau\}\hat{x} = A(\tau)\exp\{j[\omega_c\tau + \Omega(\tau)]\}\hat{x}$. The space-time variable $\tau = t - \hat{z}\cdot\mathbf{r}/c_0$ involves the position vector $\mathbf{r}$ of a field point and the phase velocity $c_0 = \frac{1}{\sqrt{\epsilon_0\mu_0}}$ of em

waves in the unbounded free space around the scatterer.

Amplitude and phase modulations are defined by $A(\tau) = \Pi\left(\frac{\tau - T/2}{T}\right)$ and $\Omega(\tau) = \pi\frac{B}{T}\left(\tau - \frac{T}{2}\right)^2$. As $\Pi\left(\frac{x-x_0}{X}\right) = 1$ or 0 for $|x - x_0| \leq$ or $> X/2$, respectively, $E(\tau) = A(\tau)\exp\{j\Omega(\tau)\}$ defines a unit-amplitude, baseband, linear chirp that modulates the carrier wave (frequency f_c). The instantaneous frequency $f(\tau) = \frac{1}{2\pi}\frac{\mathrm{d}}{\mathrm{d}\tau}\left[\omega_c\tau + \Omega(\tau)\right] = f_c + \frac{B}{T}\left(\tau - \frac{T}{2}\right)$ varies linearly from $f_c - B/2$ to $f_c + B/2$ over the time range $[0, T]$. It may be useful to note that $k_0 = \frac{\omega}{c_0} = \frac{2\pi f}{c_0}$ involves the instantaneous frequency.

The spectrum of $E(\tau)$ is formulated by use of the Fresnel integrals $C(v) = \int_0^v \cos\left(\frac{\pi}{2}\tau^2\right)\mathrm{d}\tau$, $S(v) = \int_0^v \sin\left(\frac{\pi}{2}\tau^2\right)\mathrm{d}\tau$ [26] as follows:

$$\begin{aligned} E(f) &= \frac{T}{\sqrt{2(BT)}}\left[C(v_1) + C(v_2) + jS(v_1)\right. \\ &\quad \left. + jS(v_2)\right]\exp\left\{-j\pi(BT)\frac{f}{B}\left(1 + \frac{f}{B}\right)\right\}, \end{aligned} \tag{1}$$

where $v_1 = \sqrt{\frac{BT}{2}}\left(1 - 2\frac{f}{B}\right)$, $v_2 = \sqrt{\frac{BT}{2}}\left(1 + 2\frac{f}{B}\right)$. The time-bandwidth product BT is the cardinal feature of the chirp spectrum.

3. Frequency-domain analytical formulation

Pulsed excitation calls for Fourier-transform pairs $x(t) \leftrightarrow x(\omega)$, linked through the well-known equations $x(\omega) = \int_{-\infty}^{\infty} x(t)\exp\{-j\omega t\}\mathrm{d}t$ and $x(t) = \frac{1}{2\pi}\int_{-\infty}^{\infty} x(\omega)\exp\{j\omega t\}\mathrm{d}\omega$. Thus, an em wave in region 0 is represented either by the electric-field vector $\mathbf{E}_0(\mathbf{r}, t)$, which solves the homogeneous wave equation $(\nabla^2 - c_0^{-2}\partial^2/\partial t^2)\mathbf{E}_0(\mathbf{r}, t) = 0$ [27], or by the frequency spectrum thereof $\mathbf{E}_0(\mathbf{r}, \omega) = \int_{-\infty}^{\infty}\mathbf{E}_0(\mathbf{r}, t)\exp\{-j\omega t\}\mathrm{d}t$, which solves the homogeneous Helmholtz equation $\left(\nabla^2 + k_0^2\right)\mathbf{E}_0(\mathbf{r}, \omega) = 0$.

Evidently, the very same steps that lead to the well-known time-domain extended-Mie solution of this radiation problem with time-harmonic excitation can lead to a frequency-domain solution in the case of pulsed excitation. The frequency spectrum of the electric field can be formulated as a series of spherical

eigenvectors $\mathbf{M}^{(\iota)}_{mn,s}(k\mathbf{r})$ and $\mathbf{N}^{(\iota)}_{mn,s}(k\mathbf{r})$ [28]. The symmetry index s is assigned the names e (even) or o (odd), the angular-momentum index n is assigned the integers $1, 2, \ldots$, and the azimuthal quantum number m is assigned the integers $0, 1, \ldots, n$, if $s = \mathrm{e}$, or $1, 2, \ldots, n$, if $s = \mathrm{o}$. Even-symmetry spherical eigenvectors $\mathbf{M}^{(\iota)}_{mn,\mathrm{e}}(k\mathbf{r})$, $\mathbf{N}^{(\iota)}_{mn,\mathrm{e}}(k\mathbf{r})$ are defined as follows:

$$\begin{aligned}
\mathbf{M}^{(\iota)}_{mn,\mathrm{e}}(k\mathbf{r}) &= -\hat{\theta} z^{(\iota)}_n(kr)\tau^{(1)}_{mn}(\theta)\, m\sin(m\phi) - \hat{\phi} z^{(\iota)}_n(kr)\tau^{(2)}_{mn}(\theta)\cos(m\phi), \\
\mathbf{N}^{(\iota)}_{mn,\mathrm{e}}(k\mathbf{r}) &= \hat{r}\frac{n(n+1)}{kr} z^{(\iota)}_n(kr) P^m_n(\cos\theta)\cos(m\phi) \\
&\quad + \hat{\theta}\eta^{(\iota)}_n(kr)\tau^{(2)}_{mn}(\theta)\cos(m\phi) - \hat{\phi}\eta^{(\iota)}_n(kr)\tau^{(1)}_{mn}(\theta)\, m\sin(m\phi),
\end{aligned} \tag{2}$$

$\hat{r}, \hat{\theta}, \hat{\phi}$ being unit vectors for r, θ, ϕ. Depending on the superscript ι, which is assigned the integers 1 or 2, the radial function $z^{(\iota)}_n(x)$ is either the spherical Bessel function of the 1st kind $j_n(x)$ or the spherical Hankel function of the 2nd kind $h^{(2)}_n(x)$ [26]; $\eta^{(\iota)}_n(x) = \frac{1}{x}\frac{\mathrm{d}}{\mathrm{d}x}\left[x z^{(\iota)}_n(x)\right]$ is the Riccati function that corresponds to $z^{(\iota)}_n(x)$; $P^m_n(\cos\theta)$ is an associated Legendre function of the 1st kind and $\tau^{(1)}_{mn}(\theta) = \frac{1}{\sin\theta} P^m_n(\cos\theta)$, $\tau^{(2)}_{mn}(\theta) = \frac{\mathrm{d}}{\mathrm{d}\theta} P^m_n(\cos\theta)$ are generalised Legendre functions [26, 29]. Odd-symmetry spherical eigenvectors $\mathbf{M}^{(\iota)}_{mn,\mathrm{o}}(k\mathbf{r})$, $\mathbf{N}^{(\iota)}_{mn,\mathrm{o}}(k\mathbf{r})$ may be obtained from (2) by substitution of $\sin(m\phi), \cos(m\phi)$ by $-\cos(m\phi), \sin(m\phi)$, respectively. The ensuing formulation can be made most concise by use of the notation $\mathbf{F}^{(\iota)}_{\alpha,mn,s}(k\mathbf{r})$ for the spherical eigenvectors, thereby introducing the type index $\alpha = \{\mathrm{M}, \mathrm{N}\}$. Thus, $\mathbf{F}^{(\iota)}_{\mathrm{M},mn,s} = \mathbf{M}^{(\iota)}_{mn,s}$ and $\mathbf{F}^{(\iota)}_{\mathrm{N},mn,s} = \mathbf{N}^{(\iota)}_{mn,s}$.

The spectrum of the incident electric field is formulated as follows [30]:

$$\mathbf{E}_{\mathrm{inc}}(\mathbf{r}, \omega) = -E(\omega - \omega_c)\sum_{s,nm,\alpha}(\delta_{\alpha\mathrm{M}}\delta_{s\mathrm{o}} + j\delta_{\alpha\mathrm{N}}\delta_{s\mathrm{e}})\delta_{m1} c_n \mathbf{F}^{(1)}_{\alpha,mn,s}(k_0\mathbf{r}), \tag{3}$$

where $c_n = (-j)^n \frac{2n+1}{n(n+1)}$ and $E(\omega - \omega_c)$ is the (angular frequency) spectrum of $E(\tau)$ shifted by the carrier (angular) frequency $\omega_c = 2\pi f_c$. The Kronecker delta – defined as $\delta_{xy} = 1, 0$ severally for $x = y$, $x \neq y$ – is used in (3) and extensively

throughout the ensuing analysis for conciseness. The spectrum of the scattered electric field and that of the internal electric field, may be formulated likewise:

$$\mathbf{E}_{\rm sca}(\mathbf{r},\omega) = E(\omega-\omega_c)\sum_{s,nm,\alpha} A_{\alpha,mn,s}\mathbf{F}^{(2)}_{\alpha,mn,s}(k_0\mathbf{r}),$$
$$\mathbf{E}_2(\mathbf{r}_1,\omega) = E(\omega-\omega_c)\sum_{s,nm,\alpha}\Big[B_{\alpha,mn,s}\mathbf{F}^{(1)}_{\alpha,mn,s}(k_2\mathbf{r}_1)+C_{\alpha,mn,s}\mathbf{F}^{(2)}_{\alpha,mn,s}(k_2\mathbf{r}_1)\Big]. \quad (4)$$

The overall spectrum of the external electric field is $\mathbf{E}_0(\mathbf{r},\omega) = \mathbf{E}_{\rm inc}(\mathbf{r},\omega) + \mathbf{E}_{\rm sca}(\mathbf{r},\omega)$. Both $\mathbf{E}_{\rm inc}(\mathbf{r},\omega)$ and $\mathbf{E}_{\rm sca}(\mathbf{r},\omega)$ are expressed in $(O, r\theta\phi)$. The incident field is regular at the origin and the scattered field is regular at infinity. Region 2 is confined by the spherical surfaces S_1 and S_2. The internal field consists of two parts, both expressed in $(O_1, r_1\theta_1\phi_1)$. Thus, the internal field is finite even at O, which may be exposed if $d_1 > a_1$.

The wave amplitudes $A_{\alpha,mn,s}$, $B_{\alpha,mn,s}$, and $C_{\alpha,mn,s}$ are determined by enforcement of the boundary conditions on S_1 and S_2. This is done non-locally by use of the IMM equations [11, 14, 16]:

$$\oint_{S_2}[\mathbf{E}_0\times\nabla\times\mathbf{Q}-\mathbf{Q}\times\nabla\times\mathbf{E}_0]\cdot\hat{r}\,\mathrm{d}s_2 = \oint_{S_2}[\mathbf{E}_2\times\nabla\times\mathbf{Q}-\mathbf{Q}\times\nabla\times\mathbf{E}_2]\cdot\hat{r}\,\mathrm{d}s_2,$$
$$\oint_{S_1}\mathbf{Q}\times\mathbf{E}_2\cdot\hat{r}_1\,\mathrm{d}s_1 = 0. \quad (5)$$

The auxiliary function $\mathbf{Q}$ may be replaced by a spherical eigenvector $\mathbf{F}^{(\iota)}_{\gamma,\mu\nu,\sigma}(k_2\mathbf{r})$ or $\mathbf{F}^{(\iota)}_{\gamma,\mu\nu,\sigma}(k_2\mathbf{r}_1)$, where $\gamma\in\{\mathrm{M},\mathrm{N}\}$, $\nu\in[1,\infty)$, $\mu\in[0,\nu]$, and $\sigma\in\{\mathrm{e},\mathrm{o}\}$.

The first of (5) results from the continuity of the tangential components of electric and magnetic fields across S_2. However, in order to apply the boundary condition on S_2 we must reformulate $\mathbf{E}_2(\mathbf{r},\omega)$ so that only spherical eigenvectors that are natural on S_2 are used. This is done by use of the translational addition theorem of spherical eigenvectors [31, 32, 33, 34], as formulated for the aforesaid use [24]:

$$\mathbf{F}^{(\iota)}_{\alpha,mn,s}(k_2\mathbf{r}_1) = \sum_{s',n'm',\alpha'}\mathcal{W}^{\alpha,mn,s}_{\alpha',m'n',s'}(-k_2\mathbf{d}_1)\,\mathbf{F}^{(\iota)}_{\alpha',m'n',s'}(k_2\mathbf{r}). \quad (6)$$

The coupling coefficients are concisely defined as follows:

$$\mathcal{W}^{\alpha,mn,s}_{\alpha',m'n',s'} = \Big[\delta_{\mathrm{se}}\left(\delta_{\alpha'\alpha}\hat{\mathcal{A}}^{mn}_{m'n',1}+\delta_{\alpha'\beta}\hat{\mathcal{B}}^{mn}_{m'n',1}\right)+\delta_{\mathrm{so}}\left(\delta_{\alpha'\alpha}\check{\mathcal{A}}^{mn}_{m'n',1}+\delta_{\alpha'\beta}\check{\mathcal{B}}^{mn}_{m'n',1}\right)\Big] \\ (\delta_{s'\mathrm{e}}+j\delta_{s'\mathrm{o}}) \tag{7}$$

in terms of $\hat{\mathcal{A}}^{mn}_{m'n',1}$, $\hat{\mathcal{B}}^{mn}_{m'n',1}$ and $\check{\mathcal{A}}^{mn}_{m'n',1}$, $\check{\mathcal{B}}^{mn}_{m'n',1}$, introduced in [24]. The primed indices α', m', n', s' are assigned severally the same values/names as α, m, n, s. The index $\beta \in \{\mathrm{M}, \mathrm{N}\}$ is the opposite of α (e.g., if $\alpha = \mathrm{M}$, then $\beta = \mathrm{N}$). Thus, the spectrum of the internal electric field is formulated by use of spherical eigenvectors defined in $(O, r\theta\phi)$:

$$\mathbf{E}_2(\mathbf{r},\omega) = E(\omega-\omega_c)\sum_{s,nm,\alpha}\sum_{s',n'm',\alpha'}\mathcal{W}^{\alpha',m'n',s'}_{\alpha,mn,s}(-k_2\mathbf{d}_1) \\ \Big[B_{\alpha',m'n',s'}\mathbf{F}^{(1)}_{\alpha,mn,s}(k_2\mathbf{r})+C_{\alpha',m'n',s'}\mathbf{F}^{(2)}_{\alpha,mn,s}(k_2\mathbf{r})\Big]. \tag{8}$$

Setting $\mathbf{Q} = \mathbf{F}^{(\iota)}_{\gamma,\mu\nu,\sigma}(k_2\mathbf{r})$ and by use of the formula:

$$\oint_S \mathbf{F}^{(\iota)}_{\alpha,mn,s}(k\mathbf{r})\times\mathbf{F}^{(\iota')}_{\alpha',m'n',s'}(k'\mathbf{r})\cdot\hat{r}\mathrm{d}s \quad = \\ \pi a^2(-1)^{\delta_{\alpha\mathrm{N}}}z^{(\iota)}_{\alpha,n}(ka)z^{(\iota')}_{\beta,n}(k'a)\frac{2n(n+1)}{2n+1}\frac{(n+m)!}{(n-m)!} \\ \delta_{ss'}\delta_{nn'}\left[\delta_{mm'}+(-1)^{\delta_{so}}\delta_{m0}\right]\delta_{\beta\alpha'}, \tag{9}$$

where $z^{(\iota)}_{\mathrm{M},n}(x) = z^{(\iota)}_n(x)$ and $z^{(\iota)}_{\mathrm{N},n}(x) = \eta^{(\iota)}_n(x)$, we arrive after some algebra at the first IMM equation:

$$-\left(\delta_{\alpha\mathrm{M}}\delta_{\mathrm{so}}+j\delta_{\alpha\mathrm{N}}\delta_{\mathrm{se}}\right)\delta_{m1}c_nU^{(1,\iota)}_{\alpha,n}(k_0,k_2,a_2) \\ +A_{\alpha,mn,s}U^{(2,\iota)}_{\alpha,n}(k_0,k_2,a_2)-\sum_{s',n'm',\alpha'}\mathcal{W}^{\alpha',m'n',s'}_{\alpha,mn,s}(-k_2\mathbf{d}_1) \\ \Big[B_{\alpha',m'n',s'}U^{(1,\iota)}_{\alpha,n}(k_2,k_2,a_2)+C_{\alpha',m'n',s'}U^{(2,\iota)}_{\alpha,n}(k_2,k_2,a_2)\Big] = 0. \tag{10}$$

The abbreviation $U^{(\iota,\iota')}_{\alpha,n}(k,k',a)$ is defined below:

$$
\begin{aligned}
U^{(\iota,\iota')}_{\mathrm{M},n}(k,k',a) &= \frac{2n(n+1)}{2n+1}\left[k' z^{(\iota)}_{\mathrm{M},n}(ka) z^{(\iota')}_{\mathrm{N},n}(k'a) - k z^{(\iota)}_{\mathrm{N},n}(ka) z^{(\iota')}_{\mathrm{M},n}(k'a)\right], \\
U^{(\iota,\iota')}_{\mathrm{N},n}(k,k',a) &= \frac{2n(n+1)}{2n+1}\left[k z^{(\iota)}_{\mathrm{M},n}(ka) z^{(\iota')}_{\mathrm{N},n}(k'a) - k' z^{(\iota)}_{\mathrm{N},n}(ka) z^{(\iota')}_{\mathrm{M},n}(k'a)\right].
\end{aligned} \tag{11}
$$

It may easily be verified that $U^{(\iota,\iota')}_{\mathrm{M},n}(k,k,a) = U^{(\iota,\iota')}_{\mathrm{N},n}(k,k,a)$, $U^{(\iota,\iota')}_{\alpha,n}(k,k',a) = -U^{(\iota',\iota)}_{\alpha,n}(k',k,a)$, and therefore $U^{(\iota,\iota)}_{\alpha,n}(k,k,a) = 0$.

The second of (5) results from the condition $\hat{r}_1 \times \mathbf{E}_2 = 0$, which must be imposed anywhere on S_1. Hence, $\mathbf{Q} \cdot [\hat{r}_1 \times \mathbf{E}_2] = 0 \Rightarrow [\mathbf{Q} \times \mathbf{E}_2] \cdot \hat{r}_1 = 0 \Rightarrow \oint_{S_1} \mathbf{Q} \times \mathbf{E}_2 \cdot \hat{r}_1 \mathrm{d}s_1 = 0$. If $\mathbf{Q} = \mathbf{F}^{(\iota)}_{\gamma,\mu\nu,\sigma}(k_2\mathbf{r}_1)$, we may apply (9) to arrive at the second IMM equation, which is a simple relationship between the wave amplitudes $B_{\alpha,mn,s}$, $C_{\alpha,mn,s}$:

$$
B_{\alpha,mn,s} = -\frac{z^{(2)}_{\alpha,n}(k_2 a_1)}{z^{(1)}_{\alpha,n}(k_2 a_1)} C_{\alpha,mn,s}. \tag{12}
$$

The latter, if used in (10), yields:

$$
\begin{aligned}
&-\left(\delta_{\alpha\mathrm{M}}\delta_{\mathrm{so}} + j\delta_{\alpha\mathrm{N}}\delta_{\mathrm{se}}\right)\delta_{m1} c_n U^{(1,\iota)}_{\alpha,n}(k_0,k_2,a_2) \\
&+A_{\alpha,mn,s} U^{(2,\iota)}_{\alpha,n}(k_0,k_2,a_2) - \sum_{s',n'm',\alpha'} \mathcal{W}^{\alpha',m'n',s'}_{\alpha,mn,s}(-k_2\mathbf{d}_1) \\
&C_{\alpha',m'n',s'}\left[U^{(2,\iota)}_{\alpha,n}(k_2,k_2,a_2) - \frac{z^{(2)}_{\alpha',n'}(k_2 a_1)}{z^{(1)}_{\alpha',n'}(k_2 a_1)} U^{(1,\iota)}_{\alpha,n}(k_2,k_2,a_2)\right] = 0
\end{aligned} \tag{13}
$$

and, by setting $\iota = 1$ therein, we find $A_{\alpha,mn,s}$ in terms of $C_{\alpha,mn,s}$:

$$
\begin{aligned}
A_{\alpha,mn,s} = &\left(\delta_{\alpha\mathrm{M}}\delta_{\mathrm{so}} + j\delta_{\alpha\mathrm{N}}\delta_{\mathrm{se}}\right)\delta_{m1} c_n \frac{U^{(1,1)}_{\alpha,n}(k_0,k_2,a_2)}{U^{(2,1)}_{\alpha,n}(k_0,k_2,a_2)} \\
&+ \frac{U^{(2,1)}_{\alpha,n}(k_2,k_2,a_2)}{U^{(2,1)}_{\alpha,n}(k_0,k_2,a_2)} \sum_{s',n'm',\alpha'} \mathcal{W}^{\alpha',m'n',s'}_{\alpha,mn,s}(-k_2\mathbf{d}_1)\, C_{\alpha',m'n',s'}.
\end{aligned} \tag{14}
$$

Hence, $A_{\alpha,mn,s}$ can be eliminated from (13), thus arriving at a linear equation for $C_{\alpha,mn,s}$:

$$\sum_{s',n'm',\alpha'} \mathcal{W}_{\alpha,mns}^{\alpha',m'n',s'}(-k_2\mathbf{d}_1)\left[\frac{U_{\alpha,n}^{(2,1)}(k_2,k_2,a_2)}{U_{\alpha,n}^{(2,1)}(k_0,k_2,a_2)}\right.$$
$$\left.+\frac{z_{\alpha',n'}^{(2)}(k_2a_1)}{z_{\alpha',n'}^{(1)}(k_2a_1)}\frac{U_{\alpha,n}^{(1,2)}(k_2,k_2,a_2)}{U_{\alpha,n}^{(2,2)}(k_0,k_2,a_2)}\right]C_{\alpha',m'n',s'}$$
$$=-\left(\delta_{\alpha\mathrm{M}}\delta_{s\mathrm{o}}+j\delta_{\alpha\mathrm{N}}\delta_{s\mathrm{e}}\right)\delta_{m1}c_n\left[\frac{U_{\alpha,n}^{(1,1)}(k_0,k_2,a_2)}{U_{\alpha,n}^{(2,1)}(k_0,k_2,a_2)}\right.$$
$$\left.-\frac{U_{\alpha,n}^{(1,2)}(k_0,k_2,a_2)}{U_{\alpha,n}^{(2,2)}(k_0,k_2,a_2)}\right]. \tag{15}$$

As $\alpha = \mathrm{M},\mathrm{N}$ and $s = \mathrm{e},\mathrm{o}$, the latter equation generates $2\times 2 = 4$ equations for 4 unknowns, the wave amplitudes $C_{\mathrm{M},mn,\mathrm{e}}$, $C_{\mathrm{N},mn,\mathrm{e}}$, $C_{\mathrm{M},mn,\mathrm{o}}$, $C_{\mathrm{N},mn,\mathrm{o}}$.

Actually, the index n is assigned the integers $1,2,\ldots,n_{\max}$ and the truncation number $n_{\max}$ is defined through a convergence criterion applied to a far-field observable (e.g., the mrcs). Thus, (15) generates $L_{\mathrm{e}} = n_{\max}\left(n_{\max}+3\right)$ equations with $s = \mathrm{e}$ and $L_{\mathrm{o}} = n_{\max}\left(n_{\max}+1\right)$ equations with $s = \mathrm{o}$, which is a total of $L = L_{\mathrm{e}} + L_{\mathrm{o}} = 2n_{\max}\left(n_{\max}+2\right)$ equations. The actual number of unknowns in (15) is also equal to L, because $\mathbf{F}_{\alpha,0n,\mathrm{o}}^{(\iota)}\left(k\mathbf{r}\right) = 0$ and, therefore, $A_{\alpha,0n,\mathrm{o}}$, $B_{\alpha,0n,\mathrm{o}}$, $C_{\alpha,0n,\mathrm{o}}$ do not occur in (4).

However, the $L\times L$ set of linear equations for $C_{\alpha,mn,s}$ cannot be solved unless it is decomposed into an $L_{\mathrm{e}}\times L_{\mathrm{e}}$ set of linear equations for $C_{\alpha,mn,\mathrm{e}}$ and an $L_{\mathrm{o}}\times L_{\mathrm{o}}$ set of linear equations for $C_{\alpha,mn,\mathrm{o}}$. Proof of the fact that even-symmetry wave amplitudes are decoupled from odd-symmetry ones is given in Appendix A. Herein, it suffices to present the set of equations for $C_{\alpha,mn,\mathrm{e}}$:

$$\sum_{n'm'}\left[\hat{\mathcal{A}}_{mn,1}^{m'n'}U_{\mathrm{M},n}^{\mathrm{M},n'}C_{\mathrm{M},m'n',\mathrm{e}}+\hat{\mathcal{B}}_{mn,1}^{m'n'}U_{\mathrm{M},n}^{\mathrm{N},n'}C_{\mathrm{N},m'n',\mathrm{e}}\right]=0,$$
$$\sum_{n'm'}\left[\hat{\mathcal{B}}_{mn,1}^{m'n'}U_{\mathrm{N},n}^{\mathrm{M},n'}C_{\mathrm{M},m'n',\mathrm{e}}+\hat{\mathcal{A}}_{mn,1}^{m'n'}U_{\mathrm{N},n}^{\mathrm{N},n'}C_{\mathrm{N},m'n',\mathrm{e}}\right]=-j\delta_{m1}c_nU_{\mathrm{N},n},$$
$$n,n'=1,2,\ldots,n_{\max}\qquad m,m'=0,1,\ldots,n \tag{16}$$

and the set of equations for $C_{\alpha,mn,\mathrm{o}}$:

$$\sum_{n'm'}\left[\check{\mathcal{A}}^{m'n'}_{mn,1}U^{\mathrm{M},n'}_{\mathrm{M},n}C_{\mathrm{M},m'n',\mathrm{o}}+\check{\mathcal{B}}^{m'n'}_{mn,1}U^{\mathrm{N},n'}_{\mathrm{M},n}C_{\mathrm{N},m'n',\mathrm{o}}\right]=j\delta_{m1}c_nU_{\mathrm{M},n},$$
$$\sum_{n'm'}\left[\check{\mathcal{B}}^{m'n'}_{mn,1}U^{\mathrm{M},n'}_{\mathrm{N},n}C_{\mathrm{M},m'n',\mathrm{o}}+\check{\mathcal{A}}^{m'n'}_{mn,1}U^{\mathrm{N},n'}_{\mathrm{N},n}C_{\mathrm{N},m'n',\mathrm{o}}\right]=0.$$
$$n,n'=1,2,\ldots,n_{\max}\qquad m,m'=1,2,\ldots,n \tag{17}$$

The abbreviations $U^{\alpha',n'}_{\alpha,n}$, $U_{\alpha,n}$ are defined in Appendix A.

Once $C_{\alpha,mn,s}$ are calculated from (16) and (17) by use of a computer, $A_{\alpha,mn,s}$ and $B_{\alpha,mn,s}$ are determined, severally, by use of (14) and (12). It is necessary to mention that (14) must be used under the condition $s'=s$, which had had to be imposed on (15), too, as proven in Appendix A.

3.1. Concentric inclusion

If $d_1=0$, it can be proven (see Appendix B) that $\mathcal{W}^{\alpha,mn,s}_{\alpha',m'n',s'}=\delta_{\alpha\alpha'}\delta_{mm'}\delta_{nn'}\delta_{ss'}$. By substitution into (15) we determine $C_{\alpha,mn,s}$ analytically and then $A_{\alpha,mn,s}$, $B_{\alpha,mn,s}$. The result is formulated as follows:

$$\begin{aligned}
A_{\alpha,mn,s} &= \left(\delta_{\alpha\mathrm{M}}\delta_{\mathrm{so}}+j\delta_{\alpha\mathrm{N}}\delta_{\mathrm{se}}\right)\delta_{m1}c_n \\
&\quad \frac{U^{(1,1)}_{\alpha,n}(k_0,k_2,a_2)-\frac{z^{(1)}_{\alpha,n}(k_2a_1)}{z^{(2)}_{\alpha,n}(k_2a_1)}U^{(1,2)}_{\alpha,n}(k_0,k_2,a_2)}{U^{(2,1)}_{\alpha,n}(k_0,k_2,a_2)-\frac{z^{(1)}_{\alpha,n}(k_2a_1)}{z^{(2)}_{\alpha,n}(k_2a_1)}U^{(2,2)}_{\alpha,n}(k_0,k_2,a_2)}, \\
B_{\alpha,mn,s} &= \left(\delta_{\alpha\mathrm{M}}\delta_{\mathrm{so}}+j\delta_{\alpha\mathrm{N}}\delta_{\mathrm{se}}\right)\delta_{m1}c_n\frac{1}{U^{(1,2)}_{\alpha,n}(k_2,k_2,a_2)} \\
&\quad \frac{\begin{vmatrix} U^{(1,1)}_{\alpha,n}(k_0,k_2,a_2) & U^{(1,2)}_{\alpha,n}(k_0,k_2,a_2) \\ U^{(2,1)}_{\alpha,n}(k_0,k_2,a_2) & U^{(2,2)}_{\alpha,n}(k_0,k_2,a_2)\end{vmatrix}}{U^{(2,1)}_{\alpha,n}(k_0,k_2,a_2)-\frac{z^{(1)}_{\alpha,n}(k_2a_1)}{z^{(2)}_{\alpha,n}(k_2a_1)}U^{(2,2)}_{\alpha,n}(k_0,k_2,a_2)}, \\
C_{\alpha,mn,s} &= -\frac{z^{(1)}_{\alpha,n}(k_2a_1)}{z^{(2)}_{\alpha,n}(k_2a_1)}B_{\alpha,mn,s}.
\end{aligned} \tag{18}$$

3.2. Transparent host

If $k_2=k_0$, the pec inclusion is actually free-standing. The above formulae for the wave amplitudes simplify considerably:

$$
\begin{aligned}
A_{\alpha,mn,s} &= \left(\delta_{\alpha\mathrm{M}}\delta_{so} + j\delta_{\alpha\mathrm{N}}\delta_{se}\right)\delta_{m1}c_n\frac{z^{(1)}_{\alpha,n}(k_0a_1)}{z^{(2)}_{\alpha,n}(k_0a_1)},\\
B_{\alpha,mn,s} &= -\left(\delta_{\alpha\mathrm{M}}\delta_{so} + j\delta_{\alpha\mathrm{N}}\delta_{se}\right)\delta_{m1}c_n,\\
C_{\alpha,mn,s} &= A_{\alpha,mn,s}.
\end{aligned}
\tag{19}
$$

The first of (19) is the well-known result of the Lorenz-Mie theory of scattering from a free-standing pec sphere [2, 3, 4, 25, 35, 5]. The last two of (19) manifest that the internal field is, in this marginal case, the sum of incident and scattered waves, as should have been expected for region 2, if it had had the electrical properties of free space.

3.3. Dielectric sphere without inclusion

In the absence of the inclusion, the second IMM equation is $C_{\alpha,mn,s} = 0$, instead of (12), and, thus, the first IMM equation is written as follows:

$$
\begin{aligned}
&-\left(\delta_{\alpha\mathrm{M}}\delta_{so} + j\delta_{\alpha\mathrm{N}}\delta_{se}\right)\delta_{m1}c_nU^{(1,\iota)}_{\alpha,n}(k_0,k_2,a_2)\\
&+A_{\alpha,mn,s}U^{(2,\iota)}_{\alpha,n}(k_0,k_2,a_2) - B_{\alpha,mn,s}U^{(1,\iota)}_{\alpha,n}(k_2,k_2,a_2) = 0.
\end{aligned}
\tag{20}
$$

The wave amplitudes are obtained by setting $\iota = 1, 2$ and the outcome is the well-known Lorenz-Mie result for scattering by a dielectric sphere:

$$
\begin{aligned}
A_{\alpha,mn,s} &= \left(\delta_{\alpha\mathrm{M}}\delta_{so} + j\delta_{\alpha\mathrm{N}}\delta_{se}\right)\delta_{m1}c_n\frac{U^{(1,1)}_{\alpha,n}(k_0,k_2,a_2)}{U^{(2,1)}_{\alpha,n}(k_0,k_2,a_2)},\\
B_{\alpha,mn,s} &= \left(\delta_{\alpha\mathrm{M}}\delta_{so} + j\delta_{\alpha\mathrm{N}}\delta_{se}\right)\delta_{m1}c_n\\
&\qquad\frac{\begin{vmatrix} U^{(1,1)}_{\alpha,n}(k_0,k_2,a_2) & U^{(1,2)}_{\alpha,n}(k_0,k_2,a_2)\\ U^{(2,1)}_{\alpha,n}(k_0,k_2,a_2) & U^{(2,2)}_{\alpha,n}(k_0,k_2,a_2)\end{vmatrix}}{U^{(1,2)}_{\alpha,n}(k_2,k_2,a_2)U^{(2,1)}_{\alpha,n}(k_0,k_2,a_2)}.
\end{aligned}
\tag{21}
$$

The same result can be derived from (18) in the limit $\frac{z^{(1)}_{\alpha,n}(k_2a_1)}{z^{(2)}_{\alpha,n}(k_2a_1)} \to 0$.

3.4. Transparent dielectric sphere without inclusion

In this most marginal of cases there is no scatterer in the way of the incident wave. The above formulae yield by the substitution $k_2 = k_0$:

$$\begin{aligned} A_{\alpha,mn,s} &= 0, \\ B_{\alpha,mn,s} &= -\left(\delta_{\alpha\mathrm{M}}\delta_{\mathrm{so}} + j\delta_{\alpha\mathrm{N}}\delta_{\mathrm{se}}\right)\delta_{m1}c_n. \end{aligned} \tag{22}$$

Hence, there is no scattered wave and the internal field is just the incident wave.

4. Backscattered pulse

According to (4), $\mathbf{E}_{\mathrm{sca}}(\mathbf{r},\omega)$ is formulated by use of spherical eigenvectors $\mathbf{F}^{(2)}_{\alpha,mn,s}(k_0\mathbf{r})$ which incorporate $z_n^{(2)}(k_0r)$, $\eta_n^{(2)}(k_0r)$. Because of the approximations $z_n^{(2)}(k_0r) \simeq j\eta_n^{(2)}(k_0r) \simeq j^{n+1}\frac{\exp\{-jk_0r\}}{k_0r}$, which are valid in the far field ($k_0r >> 1$) [26], the radial component of $\mathbf{F}^{(2)}_{\mathrm{N},mn,s}(k_0\mathbf{r})$ decays as $\frac{1}{(k_0r)^2}$ and, therefore, can be omitted. Furthermore, we apply the formula $\tau^{(1)}_{mnn}(\pi) = -\tau^{(2)}_{mn}(\pi) = \frac{1}{2}(-1)^n n(n+1)\delta_{m1}$ to arrive, after some algebra, at the following result for the frequency spectrum of the backscattered electric-field vector:

$$\mathbf{E}_{\mathrm{sca}}(-r\hat{z},\omega) \simeq \frac{\exp\{-j\omega r/c_0\}}{r}\mathbf{f}(-\hat{z},\omega). \tag{23}$$

The vector $\mathbf{f}(-\hat{z},\omega)$ is the frequency-domain equivalent of the backscattering amplitude [25]:

$$\mathbf{f}(-\hat{z},\omega) = \sum_n (-j)^n n(n+1)[f_{\mathrm{N},n}(\omega)\hat{x} + jf_{\mathrm{M},n}(\omega)\hat{y}], \tag{24}$$

which is formulated by use of the abbreviations:

$$\begin{aligned} f_{\alpha,n}(\omega) &= c_0\frac{A_{\alpha,n}(\omega)}{2\omega}E(\omega-\omega_c), \\ A_{\alpha,n}(\omega) &= A_{\alpha,1n,\mathrm{e}}(\omega) - jA_{\beta,1n,\mathrm{o}}(\omega). \end{aligned} \tag{25}$$

The radar observable related to backscattering is the mrcs, defined by $\sigma_{\rm mo} = 4\pi r^2 |\mathbf{E}_{\rm sca}(-r\hat{z},t)|^2$ [25], where $\mathbf{E}_{\rm sca}(-r\hat{z},t)$ is the time-domain, electric-field vector of the backscattered wave. It can easily be proven by use of (23) that:

$$\sigma_{\rm mo} \;=\; 4\pi |\mathbf{f}\left(-\hat{z}, t-r/c_0\right)|^2 \;=\; 4\pi \sum_{\alpha} \left| f_\alpha\left(\tau - 2r/c_0\right)\right|^2, \qquad (26)$$

where:

$$f_\alpha\left(t\right) \;=\; \sum_{n} (-j)^n n(n+1) f_{\alpha,n}\left(t\right) \qquad (27)$$

and $\mathbf{f}\left(-\hat{z},t\right) \leftrightarrow \mathbf{f}\left(-\hat{z},\omega\right)$, $f_{\alpha,n}\left(t\right) \leftrightarrow f_{\alpha,n}\left(\omega\right)$ are Fourier-transform pairs. It may be useful to point out that, as $\mathbf{r} = -r\hat{z}$, the space-time variable is $\tau = t + r/c_0$ and, therefore, $t - r/c_0 = \tau - 2r/c_0$. The result of (26) manifests that (a) $\sigma_{\rm mo}$ is time-dependent and (b) the backscattered pulse at r $= -r\hat{z}$ is delayed by $2r/c_0$ with respect to the incident pulse at the same point in space.

4.1. Continuous-wave excitation

The marginal case of cw excitation arises with $\mathbf{E}_{\rm inc}\left(\mathbf{r},t\right) = \exp\left\{j\omega_c t\right\}\hat{x}$, which implies that $\tau = t$, $E(\tau) = 1$, and $E(\omega) = \delta(\omega)$. Thus, (26) is simplified considerably:

$$\frac{\sigma_{\rm mo}}{\pi\alpha_2^2} = \frac{1}{x_2^2} \sum_{\alpha} \left| \sum_{n} (-j)^n n(n+1) A_{\alpha,n}(\omega_c) \right|^2 \qquad (28)$$

and $\sigma_{\rm mo}$ is, as expected, no longer dependent on the time variable. As $\sigma_{\rm mo}$ is now referenced to the geometric cross section of the scattering body, which is πa_2^2 in this paper, the formula of (28) manifests the familiar dependence of the normalized mrcs on the inverse second power of the normalized size $x_2 = \frac{\omega_c}{c_0}\alpha_2$ of the externally spherical body that gives rise to backscattering.

Concentric inclusion - transparent host. If the host is transparent and the inclusion is centred at the origin of coordinates, it may easily be verified by use of (19) that $A_{\alpha,n}(\omega_c) = -j\delta_{\alpha\mathrm{N}}c_n \left(\frac{z^{(1)}_{\mathrm{M},n}(x_1)}{z^{(2)}_{\mathrm{M},n}(x_1)} - \frac{z^{(1)}_{\mathrm{N},n}(x_1)}{z^{(2)}_{\mathrm{N},n}(x_1)}\right)$, where $x_1 = \frac{\omega_c}{c_0}a_1$ is the normalized size of the pec sphere. Thus, we readily obtain from (28) the well-known result for a free-standing pec sphere [25, 35, 5]:

$$\frac{\sigma_{\mathrm{mo}}}{\pi\alpha_1^2} = \frac{1}{x_1^2}\left|\sum_n (-1)^n(2n+1)\left(\frac{z^{(1)}_{\mathrm{M},n}(x_1)}{z^{(2)}_{\mathrm{M},n}x_1)} - \frac{z^{(1)}_{\mathrm{N},n}(x_1)}{z^{(2)}_{\mathrm{N},n}(x_1)}\right)\right|^2. \tag{29}$$

5. Outline of a Detection Scheme

The following steps are taken:

1. We plot σ_{mo} versus x_2 (or x_1) by use of (28) to find a convenient mdr (i.e., a backscattering peak) of the scattering body under cw excitation.
2. We design a linear chirp (i.e., define f_c, B, T) that targets the aforesaid mdr and then calculate the backscattered pulse by use of (26). This requires calculation of $f_{\alpha,n}(\omega)$ from (25) and use of the inverse FFT algorithm to determine $f_{\alpha,n}(t)$. Subsequently, we determine $f_\alpha(t)$ from (27) for substitution in (26).
3. We synchronise and scale $\sigma_{\mathrm{mo}}(\tau)$ for comparison with $A(\tau) = \Pi\left(\frac{\tau - T/2}{T}\right)$. The presence of a pec inclusion within the dielectric host sphere is expected to be imprinted on the shape of $\sigma_{\mathrm{mo}}(\tau)$.

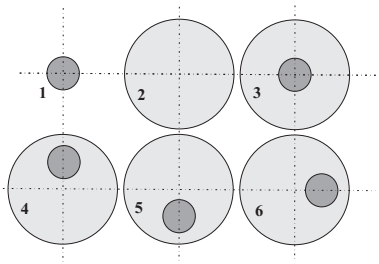

Figure 2: Dielectric sphere with pec inclusion (3-6). Marginal geometries 1,2 serve as reference.

This scheme is firstly applied to a free-standing pec sphere, then to a pec sphere placed at the center of a dielectric host sphere, and ultimately to a pec inclusion placed eccentrically within the host, as shown by Fig.2.

5.1. Free-standing pec sphere

We consider a pec sphere of radius $a_1 = 10$mm in free space. We use (29), derived from (28), to calculate the normalized mrcs – under cw excitation – versus the normalized size (Fig. 3). We target the 2nd peak that culminates at $x_1 = 2.3512$ and extends in the size range $[1.7, 3]$. The carrier frequency and the frequency span of the incident chirp are defined so that $\frac{2\pi f_c}{c_0} a_1 = 2.3512$ and $\frac{2\pi B}{c_0} a_1 = 3 - 1.7 = 1.3$. Thus, $f_c = 11.22$GHz and $B = 6.2$GHz. The spectrum of the incident chirp, shown by a blue-line plot in Fig. 3, engulfs the entire targeted mdr if the time-bandwidth product is $BT = 615$, which sets the chirp duration to $T = 99.2$ns.

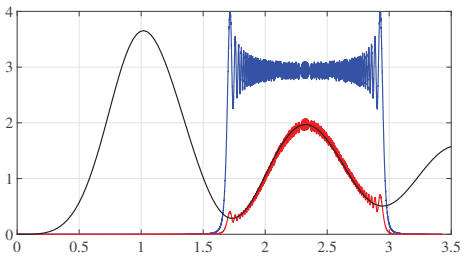

Figure 3: Free-standing, pec sphere (cw excitation): $\sigma_{\rm mo}/\pi\alpha_1^2$ versus $x_1 = \frac{2\pi f a_1}{c_0}$ (black line). Also shown (properly scaled): psd of incident chirp targeting the 2nd mdr (blue line) and psd of backscattered chirp (red line).

The time-domain mrcs $\sigma_{\rm mo}(\tau)$, which is the response of the free-standing pec sphere to the incident chirp, is shown by Fig. 4. This backscattered pulse, synchronized to the incident chirp and properly scaled, bears remarkable resemblance to the shape of the targeted mdr. Hence, the expectation that a chirp could detect the shape of an mdr is confirmed in this simple case.

It may be realised from (26) that $\sigma_{\rm mo}/4\pi = |f_{\rm M}|^2 + |f_{\rm N}|^2$. Hence, this radar observable is actually the sum of the power carried by $f_{\rm M}(\tau)$ and $f_{\rm N}(\tau)$. As

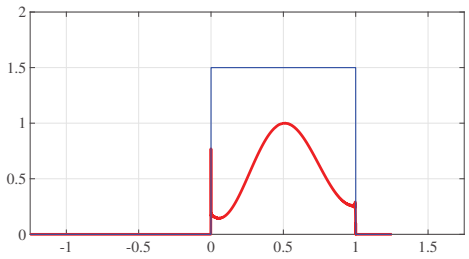

Figure 4: Free-standing, pec sphere (chirp excitation): $\sigma_{\rm mo}(\tau)$ versus τ/T (red line) and envelope of incident chirp (blue line). Plots scaled according to Fig. 3.

$f_{\rm M}(\tau) = 0$ in the case of a free-standing pec sphere, the backscattered pulse is simply $f_{\rm N}(\tau)$. The power spectral density (psd) of the latter is shown in Fig. 3 by a red-line plot. One might consider the blue-line plot as an input spectrum, the red-line plot as the output spectrum, and the black-line plot – the cw response of the free-standing pec sphere in the backscattering direction – as the transfer function, which amounts to viewing the targeted mdr as a band-pass filter.

5.2. Dielectric sphere with concentric pec inclusion

Let the aforesaid pec sphere be placed at the center of an acrylic sphere ($\mathrm{n}_2 = 1.61 - j0.004$) of radius $a_2 = 35$mm, which is approximately the size of a tennis ball. The wave amplitudes of the scattered wave are given by the 1st of (18) and the mrcs is given by (26) or (28), depending on the excitation

We compare case 3 to case 2 through Fig. 5. Black-line plots manifest the dependence of $\sigma_{\rm mo}/\pi\alpha_2^2$ on the normalised size x_2, the thinner line corresponding to case 2. Red/green plots correspond to the psd of the backscattered pulse in the presence/absence of the pec inclusion. We target the first peak of the black-line plots. If the pec inclusion is present, the targeted mdr culminates at $x_2 = 1.3$ and extends in the size range $[1.0, 1.6]$. The carrier frequency and the frequency span of the incident chirp are determined by $\frac{2\pi f_c}{c_0}a_2 = 1.3$, $\frac{2\pi B}{c_0}a_2 = 1.6 - 1.0 = 0.6$, and, thus, $f_c = 1.773$GHz, $B = 0.818$GHz. The psd

of the incident chirp (not shown) engulfs the entire targeted mdr if the time-bandwidth product is $BT = 500$, which sets the chirp duration to $T = 611$ns.

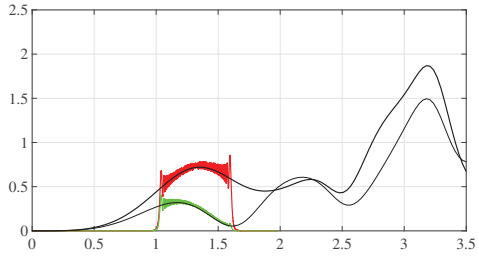

Figure 5: Dielectric sphere with concentric, pec inclusion (cw excitation): psd of backscattered chirp in the presence/absence (red/green line) of inclusion and plot of $\sigma_{\rm mo}/\pi\alpha_2^2$ vs. x_2 (black lines). The incident chirp targets the 1st mdr. The psd plots are scaled to follow the black-line plots.

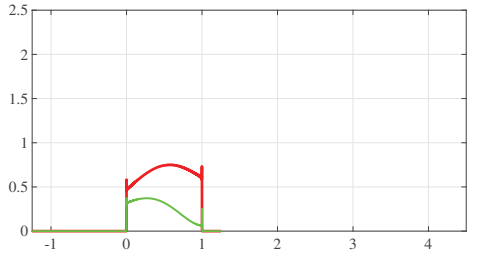

Figure 6: Dielectric sphere with concentric, pec inclusion (chirp excitation): $\sigma_{\rm mo}(\tau)$ vs. τ/T in the presence/absence of inclusion (red/green line). Plots scaled according to Fig. 5.

The psd of $f_{\rm N} - f_{\rm M}$ is absent in cases 1,2,3 – is also shown in Fig. 5, properly scaled and by use of the appropriate line color: red/green in the presence/absence of the inclusion. It is obvious that the psd follows the shape of the corresponding black-line plot. So does the time-domain backscattered pulse (Fig. 6), which proves that the inclusion can readily be detected, if the time-domain response of the dielectric sphere in the absence of the inclusion is known beforehand.

An example of improper targeting of the chirp is given by Fig. 7. As the incident chirp targets the 3rd mdr of the black-line plots in Fig. 5 , it is hardly

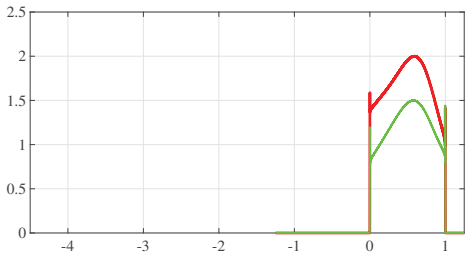

Figure 7: As Fig. 6, but targeting the 3rd mdr of Fig. 5.

possible to tell whether the pec inclusion is present or not because the backscattered pulses that correspond to cases 2 and 3 are now similar in shape. The reason is that the aforesaid, black-line plots are similar to each other in the size range $[2.5, 3.5]$.

5.3. Dielectric sphere with eccentric pec inclusion

Finally, we investigate the effect of eventual eccentricity between the dielectric host and the pec inclusion on the backscattered chirp. We start with a few checks under cw excitation.

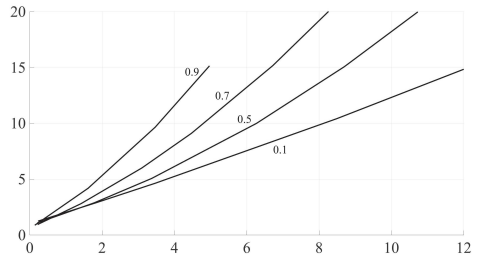

Figure 8: Dielectric sphere with eccentric, pec inclusion ($\Theta_1 = 60^o$, and $\Phi_1 = 75^o$): plots of $n_{\max}$ versus x_2. The eccentricity $d_1/d_{1,\max}$ increases from 0.1 to 0.9.

Results from a convergence check are shown in Fig. 8. Those plots are obtained by calculations of $\sigma_{\rm mo}/\pi\alpha_2^2$ over the size range $[0, 12]$ done with ever increasing truncation number $n_{\max}$. Once the eccentricity is set, iterations end when two consecutive values of the mrcs differ by less than 1%. Thus, we find

that the truncation number – the lowest integer $n_{\max}$ to achieve 1% convergence – increases dramatically with the eccentricity. Convergence is impossible with $d_1 = d_{1,\max}$, unless x_2 is negligible. The size limit for convergence is, severally, $x_{2,\max} = 5, 8, 10$, if $d_1/d_{1,\max} = 0.9, 0.7, 0.5$. The effect of eccentricity on the truncation number is symptomatic of the fact that a pec inclusion emerging from deep within the host becomes electrically dominant over the surrounding dielectric cover.

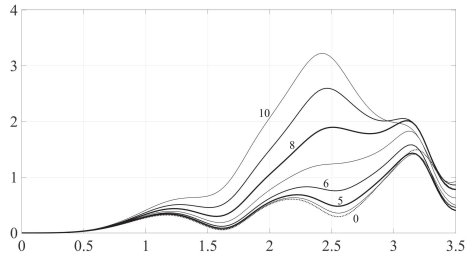

Figure 9: Dielectric sphere with shrinking, eccentric, pec inclusion ($d_1/d_{1,\max} = 0.5$, $\Theta_1 = 0^{\rm o}$, and $\Phi_1 = 0^{\rm o}$): plots of $\sigma_{\rm mo}/\pi\alpha_2^2$ (cw excitation) versus x_2. The radius a_1 of the inclusion decreases from 10mm to 0.

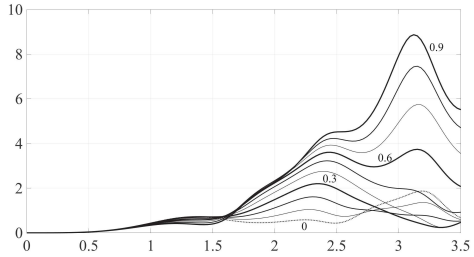

Figure 10: Dielectric sphere with diving, eccentric, pec inclusion ($a_1 = 10$mm, $\Theta_1 = 0^{\rm o}$, and $\Phi_1 = 0^{\rm o}$): plots of $\sigma_{\rm mo}/\pi\alpha_2^2$ (cw excitation) versus x_2. The eccentricity $d_1/d_{1,\max}$ decreases from 0.9 to 0.

The computer code used for cw excitation and non-zero eccentricity is validated through plots of $\sigma_{\rm mo}/\pi\alpha_2^2$ in the size range $[0, 3.5]$. Fig. 9 refers to a pec inclusion placed at $d_1 = 0.5d_{1,\max}$, $\Theta_1 = 0^{\rm o}$, $\Phi_1 = 0^{\rm o}$ and shrinking from $a_1 = 10$mm to 0, thus passing gradually from case 4 to case 2. Furthermore,

Fig. 10 refers to a case-4 pec inclusion of nominal size ($a_1 = 10$mm) which gradually dives toward the center of the host, thus ending up with the case-3 plot. The truncation number was set according to Fig. 8.

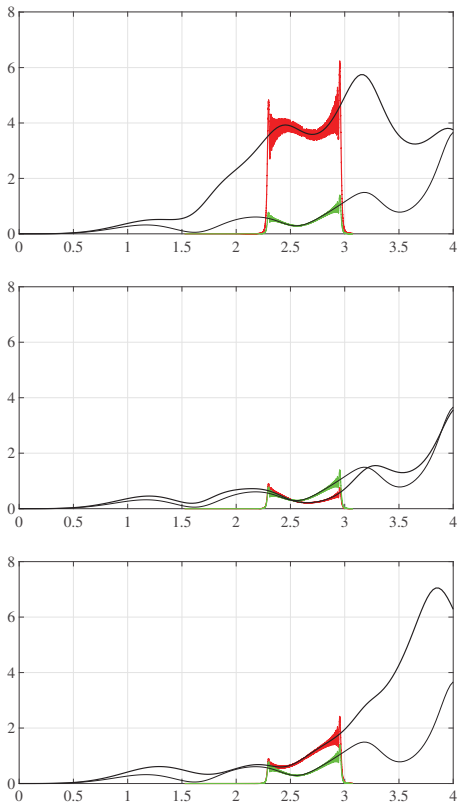

Figure 11: Dielectric sphere with eccentric, pec inclusion ($d_1/d_{1,\max} = 0.7$, $n_{\max} = 8$): plots of backscattered psd in the presence/absence (red/green line) of inclusion and $\sigma_{\rm mo}/\pi\alpha_2^2$ (cw excitation) versus x_2 (black lines). Comparison of case 4 (top), 5 (middle), and 6 (bottom) to case 2.

The final step is taken by consideration of chirp-excitation. The host ($a_2 = 35$mm) accommodates a pec inclusion ($a_1 = 10$mm) at $d_1 = 0.7d_{1,\max}$, either on the z-axis (cases 4,5) or on the x-axis (case 6). Plots of $\sigma_{\rm mo}/\pi\alpha_2^2$ (cw excitation) versus x_2 are shown by black lines in Fig. 11, the thinner line used for case 2, which is the reference (i.e., absence of inclusion). The incident chirp (not shown)

targets the size range $[2.3, 3]$. Thus, we set $f_c = 3.615GHz$, $B = 0.954$GHz, $BT = 740$, and $T = 775.7$ns. The backscattered psd is shown by a red/green line in the presence/absence of the pec inclusion. It should be noted that the red plot is the overall psd of the backscattered pulses $f_{\mathrm{M}}(\tau)$ and $f_{\mathrm{N}}(\tau)$, as both
305 are present because of non-zero eccentricity.

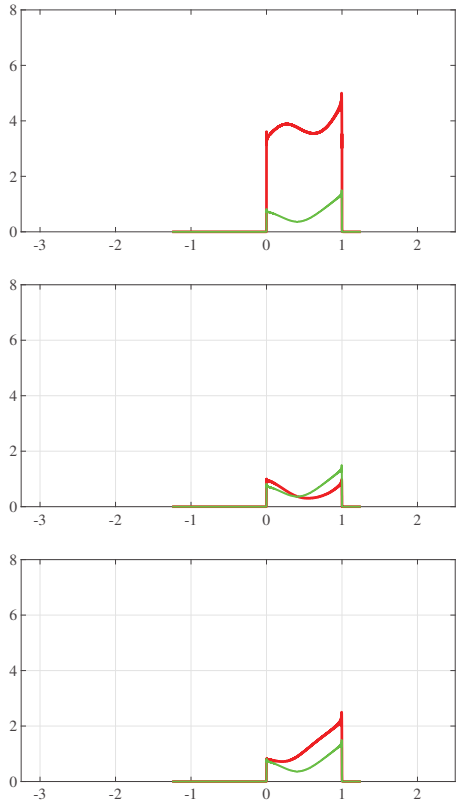

Figure 12: Plots of $\sigma_{\mathrm{mo}}(\tau)$ vs. τ/T for dielectric sphere with eccentric, pec inclusion: comparison of case 4, 5, and 6 (red line) to case 2 (green line).

The backscattered pulse is shown in Fig. 12 and, once more, it is obvious that the pulse shape is a replica of the black-line size plots (Fig. 11) within the targeted range. Moreover, case 4 emerges as the best configuration with regard to the detection of the pec inclusion. Yet, it is perhaps too soon to jump into

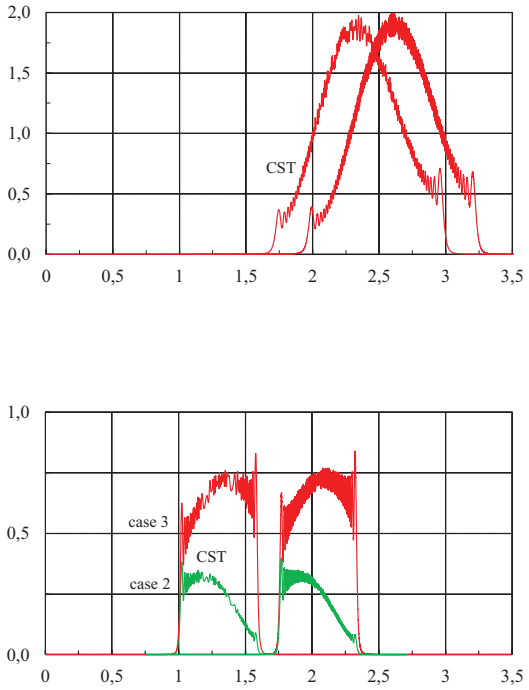

Figure 13: Plots of psd of backscattered chirp versus x_1 (top - case 1) or x_2 (bottom - cases 2,3), as determined by CST and our theory/code. The CST spectra are shown in place, whereas ours – copied from Figs. 3, 5 – are herein shifted to the right for easier inspection.

conclusions about the optimum detection scheme, as the numerical investigation of this paper is only intended to show the possibilities offered by the theory and the computer code that implements the theory.

5.4. Comparison to a commercial software

Further validation of our code – written in Fortran – is made by use of CST [36], a commercially available software. CST results are shown in Fig. 13, alongside ours, for a free-standing pec sphere (case 1), a dielectric sphere (case 2), and a dielectric sphere with a concentric metallic inclusion (case 3). The CST spectra were obtained by use of a time-domain approach based on the finite integration

technique. The simulation volume – the scattering object and part of the free space around it – was decomposed into small volume elements (up to about 200,000 of them) and it was enclosed by perfect matched layers placed.

The CST spectra of Fig. 13 are practically identical to ours, which validates both our theory and code. On closer scrutiny, the CST spectra look less smooth than ours, because the former incorporate four times less points than the latter in the size range $[0, 3.5]$, actually 1000 against 4096 points.

An interesting feature of this numerical application was our indirect way of feeding CST with an entire set of excitation frequencies in a single time simulation. If the frequency of the incident wave had been fixed, it would have been possible to select an appropriate time Gaussian excitation, which is a standard choice in the CST software. Yet, the incident chirp is actually a truncated sine wave, the frequency of which varies over a time window. Hence, we calculated the amplitude of the incident wave at each time step externally by Matlab [37] and then fed CST by those values. Because of this pre-processing of the excitation, it was possible to reduce the time required by CST to produce the entire psd of the backscattered chirp.

The CST spectra of Fig. 13 were calculated on a desktop computer with 3.20GHz Intel© Xeon© 8-core processor in about $6'$ each, which represents, roughly, $0.5'$ Matlab pre-processing and $5.5'$ CST processing. The spectra obtained by our theory/code were calculated on a laptop computer with 3.5GHz Intel Core i7 processor in less than $1''$ each. Considering that our spectra contain four times more points than the CST spectra, we realise that our code is at least 1440 times faster than CST.

6. Conclusions

The analytical formulation of this radiation problem is concise and somewhat tutorial. Originality lies with the consideration of double modulation of the wave that is incident upon the composite non-spherical body. The analytical solution successfully yields all marginal cases. The general case, implemented mainly

by purpose-made Fortran code, provides the necessary basis for the detection of a metallic object concealed in a dielectric host, both of spherical shape. It is shown that the incident chirp can target an entire mdr of the composite body and imprint the shape of that mdr on the envelope of the backscattered pulse. Moreover, the computer code yields the backscattered pulse in seconds, which is essential for design flexibility. By proper design of the incident chirp – an example is given in the numerical experiment – it is possible to detect a concealed metallic inclusion, provided that the response of the host – without the inclusion – is known. The paper focusses on the analytical formulation. The numerical application indicates the potentials of the theory and lays the way for further research, focussed on a detection scheme.

Appendix A

The generic equation (15) for the wave amplitudes $C_{\alpha,mn,s}$ can be written concisely as follows:

$$\sum_{s',n'm',\alpha'} \mathcal{W}_{\alpha,mn,s}^{\alpha',m'n',s'} U_{\alpha,n}^{\alpha',n'} C_{\alpha',m'n',s'} = -\left(\delta_{\alpha\mathrm{M}}\delta_{s\mathrm{o}}+j\delta_{\alpha\mathrm{N}}\delta_{s\mathrm{e}}\right)\delta_{m1}c_n U_{\alpha,n} \quad (30)$$

by use of the abbreviations:

$$\begin{aligned} U_{\alpha,n}^{\alpha',n'} &= \frac{U_{\alpha,n}^{(2,1)}(k_2,k_2,a_2)}{U_{\alpha,n}^{(2,1)}(k_0,k_2,a_2)} + \frac{z_{\alpha',n'}^{(2)}(k_2a_1)}{z_{\alpha',n'}^{(1)}(k_2a_1)} \frac{U_{\alpha,n}^{(1,2)}(k_2,k_2,a_2)}{U_{\alpha,n}^{(2,2)}(k_0,k_2,a_2)}, \\ U_{\alpha,n} &= \frac{U_{\alpha,n}^{(1,1)}(k_0,k_2,a_2)}{U_{\alpha,n}^{(2,1)}(k_0,k_2,a_2)} - \frac{U_{\alpha,n}^{(1,2)}(k_0,k_2,a_2)}{U_{\alpha,n}^{(2,2)}(k_0,k_2,a_2)}. \end{aligned} \quad (31)$$

According to (7), $\mathcal{W}_{\alpha,mn,s}^{\alpha',m'n',s'} = (\delta_{s\mathrm{e}} + j\delta_{s\mathrm{o}})\,\mathcal{W}_{\alpha,mn}^{\alpha',m'n',s'}$ with $\mathcal{W}_{\alpha,mn}^{\alpha',m'n',\mathrm{e}}=\delta_{\alpha\alpha'}\hat{\mathcal{A}}_{mn,1}^{m'n'}$ $+\delta_{\alpha\beta'}\hat{\mathcal{B}}_{mn,1}^{m'n'}$ and $\mathcal{W}_{\alpha,mn}^{\alpha',m'n',\mathrm{o}} = \delta_{\alpha\alpha'}\check{\mathcal{A}}_{mn,1}^{m'n'} + \delta_{\alpha\beta'}\check{\mathcal{B}}_{mn,1}^{m'n'}$. Hence, we find:

$$(\delta_{s\mathrm{e}} + j\delta_{s\mathrm{o}}) \sum_{s',n'm',\alpha'} \mathcal{W}_{\alpha,mn}^{\alpha',m'n',s'} U_{\alpha,n}^{\alpha',n'} C_{\alpha',m'n',s'} = -\left(\delta_{\alpha\mathrm{M}}\delta_{s\mathrm{o}} + j\delta_{\alpha\mathrm{N}}\delta_{s\mathrm{e}}\right)\delta_{m1}c_n U_{\alpha,n}. \quad (32)$$

The outcome is:

$$\sum_{s',n'm',\alpha'} \mathcal{W}_{\alpha,mn}^{\alpha',m'n',s'} U_{\alpha,n}^{\alpha',n'} C_{\alpha',m'n',s'} = -j\delta_{\alpha\mathrm{N}}\delta_{m1} c_n U_{\mathrm{N},n}, \tag{33}$$

if $s = \mathrm{e}$, and:

$$\sum_{s',n'm',\alpha'} \mathcal{W}_{\alpha,mn}^{\alpha',m'n',s'} U_{\alpha,n}^{\alpha',n'} C_{\alpha',m'n',s'} = j\delta_{\alpha\mathrm{M}}\delta_{m1} c_n U_{\mathrm{M},n}, \tag{34}$$

if $s = \mathrm{o}$.

If s' were allowed both names e, o in the left-hand sides of (33) and (34), the result would have been $-\delta_{\alpha\mathrm{N}} U_{\mathrm{N},n} = \delta_{\alpha\mathrm{M}} U_{\mathrm{M},n}$ or, equivalently, $U_{\alpha,n} = 0$. As the latter is wrong, so does the hypothesis that it is possible to consider $s' \neq s$ in (33) and (34). Hence, $s' = s = \mathrm{e}$ in (33), whereas $s' = s = \mathrm{o}$ in (34). The end-result is:

$$\begin{aligned} \sum_{n'm',\alpha'} \mathcal{W}_{\alpha,mn}^{\alpha',m'n',\mathrm{e}} U_{\alpha,n}^{\alpha',n'} C_{\alpha',m'n',\mathrm{e}} &= -j\delta_{\alpha\mathrm{N}}\delta_{m1} c_n U_{\mathrm{N},n}, \\ \sum_{n'm',\alpha'} \mathcal{W}_{\alpha,mn}^{\alpha',m'n',\mathrm{o}} U_{\alpha,n}^{\alpha',n'} C_{\alpha',m'n',\mathrm{o}} &= j\delta_{\alpha\mathrm{M}}\delta_{m1} c_n U_{\mathrm{M},n}. \end{aligned} \tag{35}$$

The first of (35) yields (16) by setting $\alpha = \mathrm{M}, \mathrm{N}$ and, likewise, the second yields (17).

Appendix B

Spherical eigenvectors are usually defined through the scalar eigenfunction $f_{mn}^{(\iota)}(k\mathbf{r}) = z_n^{(\iota)}(kr) P_n^m(\cos\theta) e^{jm\phi}$. Thus, $\mathbf{F}_{\mathrm{M},mn}^{(\iota)}(k\mathbf{r}) = \mathbf{M}_{mn}^{(\iota)}(k\mathbf{r}) = \nabla\times\Big(\mathbf{r} f_{mn}^{(\iota)}(k\mathbf{r})\Big)$ and $\mathbf{F}_{\mathrm{N},mn}^{(\iota)}(k\mathbf{r}) = \mathbf{N}_{mn}^{(\iota)}(k\mathbf{r}) = k\nabla\times\nabla\times\Big(\mathbf{r} f_{mn}^{(\iota)}(k\mathbf{r})\Big) = k\mathbf{F}_{\mathrm{M},mn}^{(\iota)}(k\mathbf{r})$. Even- and odd-symmetry spherical eigenvectors are obtained as follows:

$$\begin{aligned} \mathbf{F}_{\alpha,mn,\mathrm{e}}^{(\iota)}(k\mathbf{r}) &= \frac{1}{2}\left[\mathbf{F}_{\alpha,mn}^{(\iota)}(k\mathbf{r}) + (-1)^m \frac{(n+m)!}{(n-m)!}\mathbf{F}_{\alpha,-mn}^{(\iota)}(k\mathbf{r})\right], \\ \mathbf{F}_{\alpha,mn,\mathrm{o}}^{(\iota)}(k\mathbf{r}) &= \frac{1}{2j}\left[\mathbf{F}_{\alpha,mn}^{(\iota)}(k\mathbf{r}) - (-1)^m \frac{(n+m)!}{(n-m)!}\mathbf{F}_{\alpha,-mn}^{(\iota)}(k\mathbf{r})\right] \end{aligned} \tag{36}$$

and, evidently, $\mathbf{F}^{(\iota)}_{\alpha,mn}(k\mathbf{r}) = \mathbf{F}^{(\iota)}_{\alpha,mn,\mathrm{e}}(k\mathbf{r}) + j\mathbf{F}^{(\iota)}_{\alpha,mn,\mathrm{o}}(k\mathbf{r})$.

Setting $d_1 = 0$ into (7), we arrive at the following formula [24]:

$$\begin{aligned}\mathcal{W}^{\alpha,mn,s}_{\alpha',m'n',s'} = \; & \frac{1}{2}\delta_{n'n}\delta_{\alpha'\alpha}\left\{\delta_{\mathrm{se}}\left[\delta_{m'm}+(-1)^m\frac{(n+m)!}{(n-m)!}\delta_{m',-m}\right]\right. \\ & \left. - \; j\delta_{\mathrm{so}}\left[\delta_{m'm}-(-1)^m\frac{(n+m)!}{(n-m)!}\delta_{m',-m}\right]\right\}(\delta_{s'\mathrm{e}}+j\delta_{s'\mathrm{o}})\,.\end{aligned}$$

By substitution into the right-hand side of (6), we obtain, because of (36), in this marginal case:

$$\begin{aligned}\sum_{s',n'm',\alpha'}\mathcal{W}^{\alpha,mn,s}_{\alpha',m'n',s'}\mathbf{F}^{(\iota)}_{\alpha',m'n',s'}(k_2\mathbf{r}_1) \; &= \\ \frac{1}{2}\left\{\delta_{\mathrm{se}}\left[\mathbf{F}^{(\iota)}_{\alpha,mn}(k_2\mathbf{r}_1)+(-1)^m\frac{(n+m)!}{(n-m)!}\mathbf{F}^{(\iota)}_{\alpha,-mn}(k_2\mathbf{r}_1)\right]\right. & \\ \left. - \; j\delta_{\mathrm{so}}\left[\mathbf{F}^{(\iota)}_{\alpha,mn}(k_2\mathbf{r}_1)-(-1)^m\frac{(n+m)!}{(n-m)!}\mathbf{F}^{(\iota)}_{\alpha,-mn}(k_2\mathbf{r}_1)\right]\right\} \; &= \\ \delta_{\mathrm{se}}\mathbf{F}^{(\iota)}_{\alpha,mn,\mathrm{e}}(k_2\mathbf{r}_1) + \delta_{\mathrm{so}}\mathbf{F}^{(\iota)}_{\alpha,mn,\mathrm{o}}(k_2\mathbf{r}_1) \; &= \\ \mathbf{F}^{(\iota)}_{\alpha,mn,s}(k_2\mathbf{r}_1)\,, &\end{aligned}$$

which is the left-hand side of (6). Hence, $\mathcal{W}^{\alpha,mn,s}_{\alpha',m'n',s'} \equiv \delta_{\alpha\alpha'}\delta_{mm'}\delta_{nn'}\delta_{ss'}$, if $d_1 = 0$.

References

[1] M. I. Mishchenko, J. W. Hovenier, and L. D. Travis, eds., *Light scattering by nonspherical particles* (Academic, 2000).

[2] L. V. Lorenz, Lysbevaegelsen i og uden for en af plane Lysbolger belyst Kugle, Vidensk. Selsk. Skrifter **6**, 1–62 (1890).

[3] L. V. Lorenz, Sur la lumière réfléchie et réfractée par une sphere transparente, in *Œuvres scientifiques de L. Lorenz revues et annotées par H. Valentiner* (Lehmann & Stage) **1**, 403-529 (1898).

[4] G. Mie, Beiträge zur Optik trüber Medien, speziell kolloidaler Metallösungen, Annalen der Physik (Vierte Folge) **25**, 377–445 (1908).

[5] W. Hergert and T. Wriedt, eds., *The Mie theory* (Springer, 2012).

[6] J. G. Fikioris and N. K. Uzunoglou, Scattering from an eccentrically stratified dielectric sphere, J. Opt. Soc. Am. **69**, 1359–1366 (1979).

[7] F. Borghese, P. Denti, R. Saija, and O. I. Sindoni Optical properties of spheres containing a spherical eccentric inclusion, J. Opt. Soc. Am. A **9**, 1327–1335 (1992).

[8] F. Borghese, P. Denti, and R. Saija, Optical properties of spheres containing several spherical inclusions, Appl. Opt. **33**, 484–493 (1994).

[9] J. A. Roumeliotis, N. B. Kakogiannos, and J. D. Kanellopoulos, Scattering from a sphere of small radius embedded into a dielectric one, IEEE Trans. Microwave Theory Tech. **43**, 155–168 (1995).

[10] B. Miu and W. Yawei, Scattering Analysis for Eccentric-Sphere Model of Single-Nuclear Cell, in *Proceedings of Symposium on Photonics and Optoelectronics*, (2011), pp. 1–4.

[11] N. C. Skaropoulos, M. P. Ioannidou, and D. P. Chrissoulidis, Indirect mode-matching solution to scattering from a dielectric sphere with an eccentric inclusion, J. Opt. Soc. Am. A **11**, 1859–1866 (1994).

[12] M. P. Ioannidou, N. C. Skaropoulos, and D. P. Chrissoulidis, Study of interactive scattering by clusters of spheres, J. Opt. Soc. Am. A **12**, 1782–1789 (1995).

[13] N. C. Skaropoulos, M. P. Ioannidou, and D. P. Chrissoulidis, Induced EM field in a layered eccentric spheres model of the head: plane-wave and localized source exposure, IEEE Trans. Microwave Theory and Tech. **44**, 1963–1973 (1996).

[14] M. P. Ioannidou and D. P. Chrissoulidis, Electromagnetic-wave scattering by a sphere with multiple spherical inclusions, J. Opt. Soc. Am. A **19** 505–512 (2002).

[15] A. P. Moneda, M. P. Ioannidou, and D. P. Chrissoulidis, Radio-wave exposure of the human head: analytical study based on a versatile eccentric spheres model including a brain core and a pair of eyeballs, IEEE Trans. Biomedical Eng. **50**, 667–676 (2003).

[16] A. P. Moneda and D. P. Chrissoulidis, Dyadic Green's function of a sphere with an eccentric spherical inclusion, J. Opt. Soc. Am. **24**, 1695–1703 (2007).

[17] A. P. Moneda and D. P. Chrissoulidis, Dyadic Green's function of a cluster of spheres, J. Opt. Soc. Am. **24**, 3437–3443 (2007).

[18] A. P. Moneda and D. P. Chrissoulidis, Dyadic Green's function of an eccentrically stratified sphere, J. Opt. Soc. Am. A **31**, 510–517 (2014).

[19] M. Kahnert, Numerical solutions of the macroscopic Maxwell equations for scattering by non–spherical particles: A tutorial review, J. Quant. Spectrosc. Radiat. Transfer **178**, 22–37 (2016).

[20] E. E. M. Khaled and A. B. Alhasan, Temporal behavior of short optical pulses scattered by small particles, Physica Scripta **54**, 525–529 (1996).

[21] G. Gouesbet and G. Gréhan, Generic formulation of a generalized Lorenz-Mie theory for a particle illuminated by laser pulses, Part. Part. Syst. Charact. **17**, 213–224 (2000).

[22] Y. P. Han, L. Méès, K. F. Ren, G. Gréhan, Z. S. Wu, and G. Gouesbet, Far scattered field from a spheroid under a femtosecond pulsed illumination in a generalized Lorenz-Mie theory framework, Optics Communications **231**, 71–77 (2004).

[23] L. Méès, G. Gouesbet, and G. Gréhan, Transient internal and scattered fields from a multi-layered sphere illuminated by a pulsed laser, Optics Communications **282**, 4189–4193 (2009).

[24] F. P. Vervelidou and D. P. Chrissoulidis, Scattering of a pulsed wave by a sphere with an eccentric spherical inclusion, J. Opt. Soc. Am. A **29**, 605–616 (2012).

[25] A. Ishimaru, *Wave propagation and scattering in random media, Vol. I* (Academic, 1978).

[26] M. Abramowitz and I. A. Stegun, *Handbook of mathematical functions* (Dover, 1972).

[27] J.A. Stratton, *Electromagnetic theory* (McGraw-Hill, 1941).

[28] P. M. Morse and H. Feshbach, *Methods of theoretical physics, part II* (McGraw-Hill, 1864–1867, 1953).

[29] I. S. Gradshteyn and I. M. Ryzhik, *Table of integrals, series and products* (Academic, 1980).

[30] J.D. Jackson, *Classical electrodynamics* (Wiley, 1975).

[31] S. Stein, Addition theorems for spherical vector wave functions, Q. Appl. Math. **19**, 15–24 (1961).

[32] O. R. Cruzan, Translational addition theorems for spherical vector wave functions, Q. Appl. Math. **20**, 33–40 (1962).

[33] J. D. Kanellopoulos and J. G. Fikioris, Resonant frequencies in an electromagnetic eccentric spherical cavity," Q. Appl. Math. **37**, 51–66 (1979).

[34] Y. L. Xu, "Efficient evaluation of vector translation coefficients in multiparticle light-scattering theories, J. Comp. Physics **139**, 137–165 (1998).

[35] C. F. Bohren and D. R. Huffman, *Absorption and scattering of light by small particles* (Wiley, 1983).

[36] CST MWS: Computer Simulation Technology Microwave Studio, Computer Simulation Technology, Inc., Framingham, MA, 2019.

[37] MATLAB Optimization Toolbox (R2017b), The MathWorks, Inc., Natick, MA, 2017.